MOLECULAR TOXICOLOGY

CrossMark

Acetaminophen cytotoxicity in HepG2 cells is associated with a decoupling of glycolysis from the TCA cycle, loss of NADPH production, and suppression of anabolism

Volker Behrends[1] · Guro F. Giskeødegård[2] · Natalia Bravo-Santano[1] · Michal Letek[1] · Hector C. Keun[3]

© The Author(s) 2018

Abstract

Acetaminophen (APAP) is one of the most commonly used analgesics worldwide, and overdoses are associated with lactic acidosis, hepatocyte toxicity, and acute liver failure due to oxidative stress and mitochondrial dysfunction. Hepatoma cell lines typically lack the CYP450 activity to generate the reactive metabolite of APAP observed in vivo, but are still subject to APAP cytotoxicity. In this study, we employed metabolic profiling and isotope labelling approaches to investigate the metabolic impact of acute exposure to cytotoxic doses of APAP on the widely used HepG2 cell model. We found that APAP exposure leads to limited cellular death and substantial growth inhibition. Metabolically, we observed an up-regulation of glycolysis and lactate production with a concomitant reduction in carbon from glucose entering the pentose-phosphate pathway and the TCA cycle. This was accompanied by a depletion of cellular NADPH and a reduction in the de novo synthesis of fatty acids and the amino acids serine and glycine. These events were not associated with lower reduced glutathione levels and no glutathione conjugates were seen in cell extracts. Co-treatment with a specific inhibitor of the lactate/H$^+$ transporter MCT1, AZD3965, led to increased apoptosis in APAP-treated cells, suggesting that lactate accumulation could be a cause of cell death in this model. In conclusion, we show that APAP toxicity in HepG2 cells is largely independent of oxidative stress, and is linked instead to a decoupling of glycolysis from the TCA cycle, lactic acidosis, reduced NADPH production, and subsequent suppression of the anabolic pathways required for rapid growth.

Volker Behrends and Guro F. Giskeødegård have equally contributed to this work.

✉ Volker Behrends
  volker.behrends@roehampton.ac.uk

✉ Hector C. Keun
  h.keun@imperial.ac.uk

[1] Health Science Research Centre, Department of Life Sciences, University of Roehampton, London, UK

[2] Department of Circulation and Medical Imaging, Faculty of Medicine and Health Sciences, The Norwegian University of Science and Technology (NTNU), Trondheim, Norway

[3] Department of Surgery and Cancer, Faculty of Medicine, Imperial College London, London, UK

Introduction

Acetaminophen (APAP, paracetamol, or *N*-acetyl-*p*-aminophenol) is one of the world's most commonly used drugs due to its antipyretic and analgesic properties. While it is widely used and generally safe to take at low dosage (the FDA-approved dose is less than 4 g per person per day), APAP is also the world's leading cause of drug overdose and acute liver failure, with a number of these episodes being attributed to unintentional overdosing on APAP/opioid combination analgesics (Bunchorntavakul and Reddy 2013; Yoon et al. 2016).

Hepatotoxicity and necrotic liver tissue damage following overdoses are due to reactive metabolites produced from APAP in the liver. The overwhelming majority of ingested APAP is metabolised via phase II metabolism (McGill and Jaeschke 2013). At therapeutic doses, about 50–70% of APAP is glucoronidated [mainly via UGT1A1 and/ or UGT1A6 (McGill and Jaeschke 2013)] and 25–35% is

sulphated via enzymes of the SULT1 family to be excreted in urine (Coen 2015). The remaining 5–15% are oxidised to the highly reactive *N*-acetyl-*p*-benzoquinone imine (NAPQI) by the P450 enzymes, mainly CYP2E1 (Dai and Cederbaum 1995).

NAPQI readily binds sulfhydryl groups, such as in glutathione (GSH). At therapeutic doses, GSH-mediated detoxification prevents NAPQI build-up. Following over-doses, however, the GSH pool is depleted, leading to NAPQI binding of other proteins and protein damage. While NAPQI protein binding has also been observed at therapeutic doses in vitro, GSH depletion is still regarded as a pre-requisite for hepatotoxicity of APAP. This is further corroborated by the fact that *N*-acetyl cysteine (NAC), a GSH precursor, is one of the most effective acute treatments that can rescue APAP toxicity and works as an antidote in vivo if given early (McGill and Jaeschke 2013; Coen 2015).

Mechanistically, a growing body of evidence suggests that NAPQI-mediated APAP toxicity targets mitochondrial proteins (Hinson et al. 2010), potentially reducing respiration and inducing further oxidative stress, even though the exact mechanism is not yet understood. Down-stream, the relative loss of mitochondrial function and other knock-on effects, e.g., peroxynitrile-induced toxicity, lead to JNK/Alf-mediated necrosis in the liver (Hinson et al. 2010; Jaeschke et al. 2012).

Interestingly, this necrotic pathway is not seen in hepatoma lines like HepG2. HepG2 cells are an established, often used model of liver toxicity (Dai and Cederbaum 1995; Gerets et al. 2012; Jaeschke et al. 2012; Ramirez et al. 2017) studies, but have very low CYP2E1 activity (Jaeschke et al. 2012; Ramirez et al. 2017), and thus, comparatively little NAPQI is formed in response to APAP dosage. There-fore, while HepG2 cells still die after high APAP exposure (Manov et al. 2002, 2004; Macanas-Pirard et al. 2004), albeit at higher concentrations than primary cells (Raza and John 2015), they do so via caspase-mediated apoptosis, not necrosis (Jaeschke et al. 2012; McGill and Jaeschke 2013). Furthermore, it has been shown that NAC treatment does not fully rescue HepG2 cells, though there is some evidence for GSH depletion after dosing (Manov et al. 2004). As these findings point towards a different trigger for APAP-induced cell death in hepatoma lines, we were interested in investi-gating the biochemical changes following exposure.

In this study, we subjected HepG2 cells to acute high doses of APAP and compared cell viability, the changes in the intra- and extra-cellular metabolome, as well as carbon flux to that of unexposed controls. We found that short-term, high-level exposure leads to pronounced changes in the metabolism of the cells, most notably a shift away from fatty acid synthesis towards glycolysis and lactate produc-tion. We showed that, while the reduced glutathione pool was not depleted, NADPH levels decreased sharply upon the

APAP exposure. Based on our findings, we investigated the effect of co-exposure of APAP with AZD3965, an inhibitor of monocarboxylate transporter 1 (MCT1, *SLC16A1*), a key co-exporter of H^+ and lactate (Noble et al. 2017). Co-dosing with AZD3965 produced synergistic effects on apoptosis, suggesting that APAP-induced cell death in HepG2 cells may be related to lactate production and increased risk of intracellular acidosis.

Methods

Cell culture

HepG2 cells were cultured in DMEM (Gibco), and sup-plemented with 10% dialysed fetal bovine serum (FBS), 5% non-essential amino acids, 1% penicillin/streptomycin, 5.6 mM glucose, and 2 mM L-glutamine. Cells were cultured as a monolayer at 37 °C in a humidified atmosphere with 5% CO_2 under normal oxygen conditions. The cells were passaged every 2–3 days. Only low passage cells, less than 15 passages from the state when these were purchased were used for experiments.

Toxicity assays

APAP was dissolved and diluted with the appropriate media, depending on the type of experiment (see below—metabo-lomic experiments). For some experiments, we additionally dosed cells with 20 mM valproic acid, 10 μM methotrexate (in 0.1% DMSO), or 0.1% DMSO as control. To ascertain cell survival, cell activity and flow cytometry were used.

Flow cytometry

HepG2 cells were seeded in 96-well plates (Sarstedt) in DMEM and at a cell density of 3.5×10^4 cells per well. Media in each well were supplemented with the appropri-ate concentration of APAP and/or AZD3965 (see Table 1). Host cell viability was tested at 24 and 48 h after treatment. To recover both necrotic and apoptotic cells, the 96-well plates were centrifuged at 400×*g* for 10 min and supernatant was discarded. Cells were trypsinized for 5 min at 37 °C, diluted in DMEM, and centrifuged at 400×*g* for 10 min. Supernatant was again discarded. Afterwards, each sample was double stained in 25 μl of DMEM-containing 1.25 μl of annexin V-FITC and 2.5 μl of propidium iodide (PI) (Bec-ton Dickinson, BD) and incubated at room temperature for 15 min. Finally, samples were diluted with 100 μl of DMEM and host cell viability was measured by flow cytom-etry (BD Accuri™ C6 Plus). To assess cell viability and cell death, 5000 events were recorded by flow cytometry to calculate the percentage of each cell population. Based on

their forward and side scatter properties (FSC and SSC, see Fig. S1), percentages of live (higher FSC, lower SSC) and dead (lower SSC, higher FSC) cells were calculated among the whole-cell population. Annexin V/PI staining was used to detect apoptotic and necrotic cells, where Annexin V +/PI − cells are considered the early apoptotic and Annexin V +/PI + cells are considered necrotic or late apoptotic.

Sampling and extraction for metabolomics experiments

For toxicity metabolomics experiments, cells were trypsinised and re-suspended in full medium; 250,000 cells were seeded per well on a 6-well plates and allowed to adhere over-night. The medium was aspirated the next day (24 h after seeding) and was replaced with the experimental culture media, and cells were allowed to equilibrate for 1 h in DMEM (Gibco), and supplemented with 10% dialysed fetal bovine serum (FBS), 1% penicillin/streptomycin, 5.6 mM glucose, and 2 mM L-glutamine before change of media and addition of APAP. The media composition was modified to introduce either 5.6 mM U-$^{13}C_6$-glucose, 5.6 mM 1,2-$^{13}C_2$-glucose, or 2 mM $^{13}C_5$-glutamine as carbon sources depending which fluxes were investigated. All experiments were performed as independent biological triplicates.

The samples were harvested after 6 h. The media were collected and immediately placed on ice. The cell monolayer was washed with 500 µl of cold (4 °C) Ringer's solution, which was aspirated before the addition of 750 µl of cold methanol (− 20 °C). The methanol-quenched cells were then scraped from the surface of the well and the entire sample was transferred to a clean 2 ml tube. To increase metabolite recovery, each well was washed with a further 750 µl of cold methanol and pooled with the first sample. The methanol-quenched samples were dried down in a vacuum concentrator (SpeedVac). For the extracellular media samples, 1 ml of the culture media were transferred to fresh Eppendorf tubes and centrifuged (8000×g, 5 min) to remove potential cell debris. Dried down cell samples and media were stored at − 80 °C until further use.

A dual-phase methanol/chloroform extraction was used to recover aqueous metabolites and non-polar metabolites from the samples. Metabolites were extracted from the dried extracts and the samples were kept on ice during the extraction. 300 µl of chloroform/methanol in a 2:1 ratio was added to crude extract and the sample was mixed by vortexing. Then, 300 µl of UPLC grade H_2O were added (giving a final chloroform:methanol:water ratio of 2:1:3), vortexing was repeated and the sample was centrifuged at 16,000×g for 5 min. Upper aqueous fraction and lower organic fraction were transferred to separate silanized

GC–MS vials and the procedure repeated on the remaining interphase to ensure maximum yield.

Nuclear magnetic resonance spectroscopy

420 µl of culture medium, 120 µl of 1 mM 4,4-dimethyl-4-silapentane-1-sulfonic acid (DSS) in deuterium oxide (D_2O) as an internal standard, and 60 µl of 500 mM phosphate buffer, pH 7 were mixed and transferred to 5 mm glass NMR tubes for analysis. High-resolution ^{1}H NMR spectra of cell culture media were acquired at 14.1 T (600.13 MHz ^{1}H frequency) using a Bruker AVANCE 600 spectrometer (Bruker, Rheinstetten, Germany), equipped with a 5 mm inverse probe. Proton spectra were acquired following the approach described previously (Beckonert et al. 2007). Briefly, a one-dimensional NOESY pulse sequence was used for water suppression; data were acquired into 32 K data points over a spectral width of 12 kHz, with eight dummy scans and 128 scans per sample, and an additional longitudinal relaxation recovery delay of 3.5 s per scan, giving a total recycle time of 5 s. Carbon spectra were acquired using a one-dimensional pulse sequence with power-gated decoupling (zgpg pulse sequence) into 65,536 data points, with 640 scans per sample.

Gas chromatography–mass spectrometry

Dried aqueous extracts were supplemented with 10 µl of 1.5 mg/ml myristic acid-d27 as an internal standard, and the samples were dried down using a vacuum concentrator (SpeedVac). Derivatisation of unlabelled samples followed a two-step process described previously (Kind et al. 2009). First, samples were derivatised with methoxyamine. To this end, 20 µl of 20 mg/ml methoxyamine (in anhydrous pyridine) were added to samples, samples were mixed and quickly centrifuged, followed by incubation for 90 min at 30 °C. Afterwards, samples were silylated by adding 80 µl MSTFA (with 1% TMCS, Thermo) and incubated for 45 min at 37 °C. For samples derived from media containing ^{13}C glucose or ^{13}C glutamine, methoxamation was followed by silylation by adding 80 µl of MTBSTFA (with 1% TBDMS, Thermo) and incubation for 60 min at 70 °C. After incubation, samples were cooled and centrifuged. Finally, the samples were transferred to de-activated glass vial inserts prior to injection.

Dried organic extracts supplemented with 10 µl of 1.5 mg/ml myristic acid-d27 as an internal standard were dried down using a vacuum concentrator before lipid-bound fatty acids were trans-esterified. To this end, samples were reconstituted in 333 µl of methanol/toluene solution (1:1 v/v ratio), and treated with 167 µl of 0.5 M sodium methoxide and incubated at room temperature for 1 h. Reaction was halted by the addition of 500 µl of 1 M NaCl and 25 µl

of concentrated HCl. The methylated fatty acids were liquid–liquid extracted using two volumes of hexane (500 µl), and the combined organic layers were dried under N_2. Samples were reconstituted with 40 µl acetonitrile, free fatty acids silylated by adding 40 µl of MSTFA (with 1% TMCS) (Thermo) and incubated for 30 min at 37 °C. Finally, the samples were then transferred to de-activated glass vial inserts prior to injection.

GC–MS analysis was performed on an Agilent 7890 GC system connected to an Agilent 5975 MSD operating under electron impact ionization (Agilent Technologies). Metabolites were separated with a 30 m DB-5MS capillary column with an attached 10 m Duraguard column. Samples were injected with an Agilent 7693 autosampler injector into de-activated split-less liners using helium as the carrier gas at a flow rate of 1 ml/min. The chromatography parameters were based on the Fiehn method (Kind et al. 2009).

Data analysis

NMR spectra were apodized (0.5 Hz), Fourier transformed, followed by phase and baseline correction in iNMR 3.6 (Mestrelab). The data were then exported as full-resolution spectra to Matlab 2014b (Mathworks) for the further analysis using integration scripts written by the authors. We assigned metabolites by comparison of the chemical shift and multiplicity of resonances with internal and online databases (Wishart et al. 2007). Signal intensities were normalised to DSS.

GC–MS data were processed using the current version of the MATLAB-based pipeline Gavin (Behrends et al. 2011). Briefly, spectra derived from unlabelled samples were processed through the deconvolution software AMDIS (Stein 1999), using the Fiehn library as database (Kind et al. 2009), and raw data and AMDIS output files were imported into Gavin for semi-automated curation and backfilling of the integrated data matrix. Metabolite levels were normalised to cell number. For ^{13}C labelled spectra, in-house retention and mass spectral information were used for import and automated natural isotope correction [based on ref. (Millard et al. 2012)] was carried out for integrated metabolites. For *trans*-esterified fatty acids, the mass isotopologue distribution (MID) vectors were normalised and isotopomer spectral analysis applied using the ConvISA algorithm (Tredwell and Keun 2015).

Results

To assess toxicity of APAP to HepG2 cells, we carried out a high-dose short-exposure experiment. As previously reported (Manov et al. 2002, 2004; Macanas-Pirard et al. 2004), APAP is toxic and results in cell death in HepG2 cells with toxicity showing a clear concentration dependence and a clear drop in cell viability is visible in the low mM range (24 h exposure, Fig. 1a, Fig. S1). Moreover, we observed that APAP also leads to severe growth arrest in vitro, with a little detectable proliferation from 2 mM APAP upwards (Fig. 1b). We quantified the extra-cellular concentration of lactate, a readout for glycolytic rate or the Warburg effect which is a fundamental hallmark of cancer cells including hepatoma (Hanahan and Weinberg 2011). We observed significantly higher overall extra-cellular accumulation of lactate in the APAP-treated samples (Fig. 1c, $p < 10^{-4}$ in all comparisons, Student's t test). Interestingly, APAP-treated samples did not fit the inverse linear relationship of glucose consumption and lactate accumulation, observed in HepG2 cells under basal conditions or when exposed to other hepatotoxicants, using doses corresponding to LC10 (Fig. 1d). These data pointed to rearrangements in intracellular metabolite flux, which we analysed by GC/MS and ^{13}C stable isotope tracers.

We performed a dual-phase extraction to profile aqueous soluble as well as non-polar metabolites from HepG2 extracts (Fig. 2). To assess changes in flux, we labelled the cells with U-^{13}C glucose or U-^{13}C glutamine and calculated the fraction of label found in each metabolite for each condition. We also quantified relative changes in metabolite pool size as a further indication of pathway perturbation. For central carbon metabolism, our data showed that glycolytic metabolites, as expected, were almost exclusively derived from glucose (Fig. 2a). While labelling patterns from these metabolites were relatively stable with treatment, there was a sharp decrease in pool size for 3-phosphoglycerate, phosphoenolpyruvate, and pyruvate, while the intracellular levels of lactate were increased consistent with the higher production of this end product.

This shift towards higher lactate production in the presence of APAP implied a loss of entry of pyruvate into other pathways such as the TCA cycle. In control HepG2 cells, we detected high levels of m_{+2} and m_{+5} isotopologues of citrate in the presence of $^{13}C_6$ glucose, demonstrating that under basal conditions pyruvate entry into the TCA cycle was via both pyruvate dehydrogenase and the anaplerotic pathway, pyruvate carboxylase (Fig. 2b). As can be seen from Fig. 2, the proportion of glucose-derived carbon in TCA cycle intermediates was significantly reduced from 29 to 49% in control samples to 6–19% in APAP-treated samples. In citrate, the effect was particularly pronounced with both ^{13}C labelling from glucose and glutamine falling from 38 to 18%, respectively, to below < 10% in both cases (Fig. 2b, c). This confirmed that pyruvate entry into the TCA cycle and subsequent mitochondrial citrate production via citrate synthase flux had significantly decreased with APAP exposure. The overall labelling pattern for alpha-ketoglutarate, malate, and fumarate shifted from glucose and
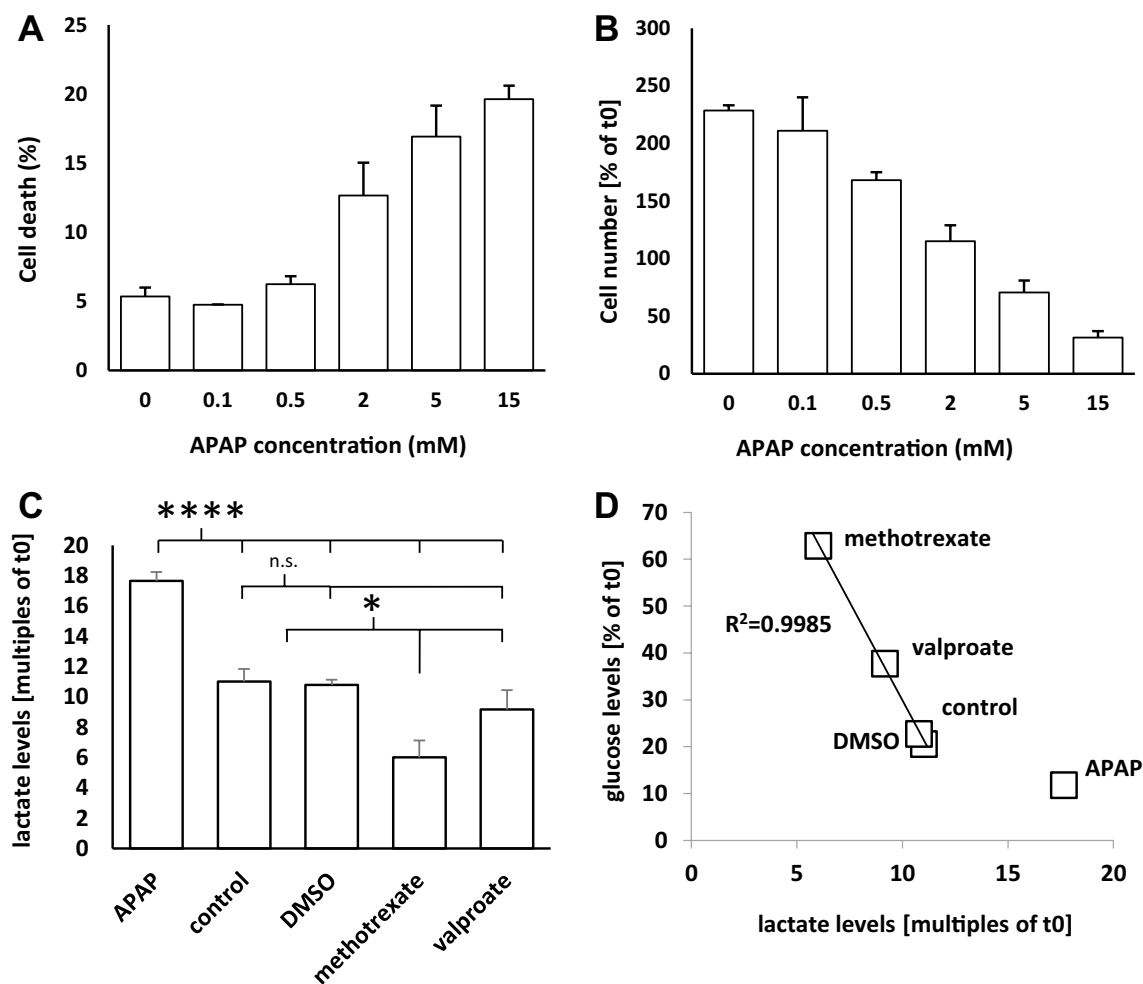
Fig. 1 APAP exposure leads to growth inhibition, cell death, and increased lactate production in HepG2 cells **a** Total cell viability, measured by flow cytometry in response to the indicated doses of APAP after 24 h exposure. Error bars indicate SE of four biological replicates. **b** Cell number, relative to initial number at time 0 h. **c** Lactate levels in media from untreated cells and cells treated with indicated toxins for 24 h. ****$p < 0.00001$ in all comparison of APAP-treated to other conditions, *n.s.* not significant, *$p < 0.01$ for all comparisons, all $n = 4$. **d** Graph showing the relationship between medium glucose and lactate levels for the different treatments

glutamine carbon contributing nearly 40% each in control samples to $^{13}C_5$ glutamine contributing more than half and ^{13}C glucose only about one-fifth in the APAP-dosed samples (Fig. 2). These intermediates can be labelled from ^{13}C glutamine in the absence of citrate oxidation via a truncated TCA cycle. The comparatively low abundance of m_{+3} isotopologues in—for example—fumarate after APAP exposure indicated that anaplerotic labelling from $^{13}C_6$ glucose after APAP treatment via pyruvate carboxylase and reverse flux of malate dehydrogenase and fumarate hydratase (Fig. S2) is minimal. Pool sizes of TCA metabolites remained relatively stable with the exception of malate which was reduced. Pool sizes of glutamine, asparagine, and aromatic amino acids (not shown) were increased. This was consistent with the suppression of the canonical TCA cycle and citrate synthesis by APAP.

Citrate plays an important anabolic role in rapidly dividing cells as is exported from the mitochondria to generate cytosolic acetyl-CoA (AcCoA) for de novo lipid (fatty acid) biosynthesis. To investigate the impact of APAP on this pathway, we carried out ISA on the organic fraction of the HepG2 extracts (Tredwell and Keun 2015) (Fig. 3). In agreement with our labelling data for TCA metabolites, we found that glucose contribution to the lipogenic AcCoA pool was dramatically reduced (Fig. 3b, c). While nearly 70% of labelled AcCoA was derived from glucose in the control samples, this fraction dropped to under 40% in APAP-treated cells. Conversely, the glutamine-derived fraction increases from around 25–45% (Fig. 3b, c). In both cases, however, the ISA model predicted a sharp decrease in de novo synthesis of lipids and fatty acids upon treatment (Fig. 3b, c). We also observed a reduction in other anabolic pathways, such as de
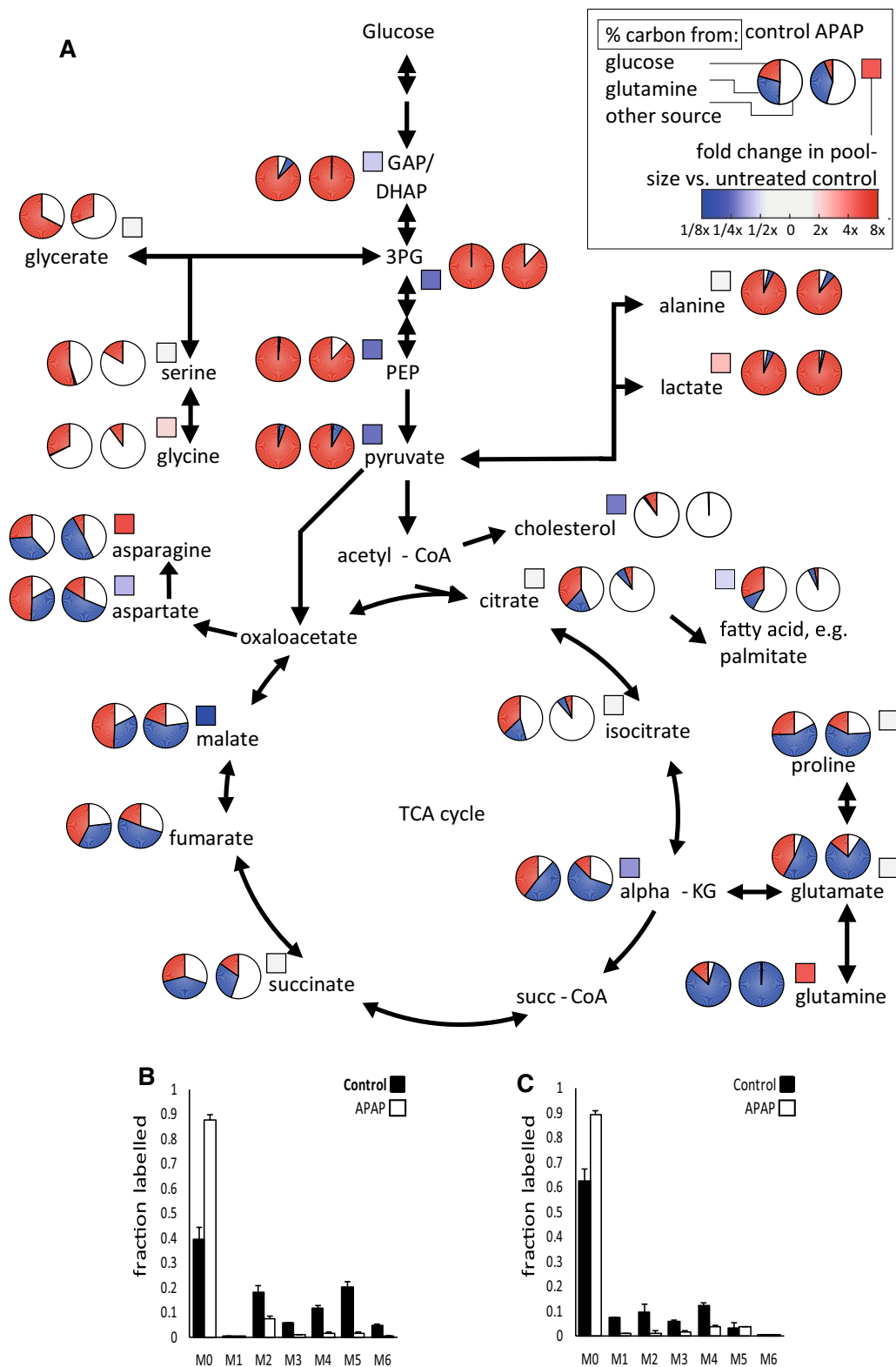
novo synthesis of serine and glycine from glucose (Fig. 2; Fig S3/S4). Collectively, these data suggest that a block on anabolism, consistent with a substantive reduction in

proliferation, is a major metabolic consequence of APAP exposure in HepG2 cells.

Fatty acid synthesis is dependent on NADPH, which is also essential for the recycling of oxidised glutathione

◄**Fig. 2** APAP decouples glycolysis from the TCA cycle and anabolism in HepG2 cells. **a** Relative contribution of glucose or glutamine carbon-to-metabolite pools are shown as carbon atom-weighted labelling percentages. The pie charts (right: APAP; left: control) show the percent of carbon in the compound originating from glucose (in red), glutamine (in blue), or other sources (in white). The coloured squares represent the fold change in metabolite level between treated compared to untreated controls, where the colour is the magnitude of effect as indicated by the colour bar (**b**) relative abundance of isotopologues of citrate in control and APAP-treated cultures labelled with U-^{13}C Glucose. **c** Relative abundance of isotopologues of citrate in control and APAP-treated cultures labelled with U-^{13}C Glutamine. Errors bars represent S.E., all experiment $n = 3$. (Color figure online)

(Vander Heiden et al. 2009; Currie et al. 2013) during oxidative stress. Therefore, we investigated the significance of APAP-induced changes in glucose and mitochondrial metabolism on NADPH status. We found that, while total NADP(H) was increased in treated cells, the fraction of

NADPH was sharply reduced after treatment implying possible oxidative stress ($p < 0.05$, Student's t test, Fig. 4a). In contrast, total glutathione increased ($p < 0.05$, Student's t test) in treated cells, while oxidised glutathione remained unchanged ($p = 0.83$, Student's t test, Fig. 4b). Furthermore, no evidence for GSH-conjugated APAP metabolites or mercapturates could be found in extracts assayed by NMR spectroscopy (data not shown). These would be expected if APAP was being activated to electrophilic metabolites such as NAPQI that are associated with the oxidative stress induced in the liver by APAP toxicity. Thus, we concluded that the loss of NADPH was not likely to be due to oxidative stress, but possibly reduced generation of NADPH.

The pentose-phosphate pathway (PPP), which diverts metabolites from glycolysis, is a major source of cellular NADPH generation and recycling (Vander Heiden et al. 2009; Stincone et al. 2015). Hence, we quantified
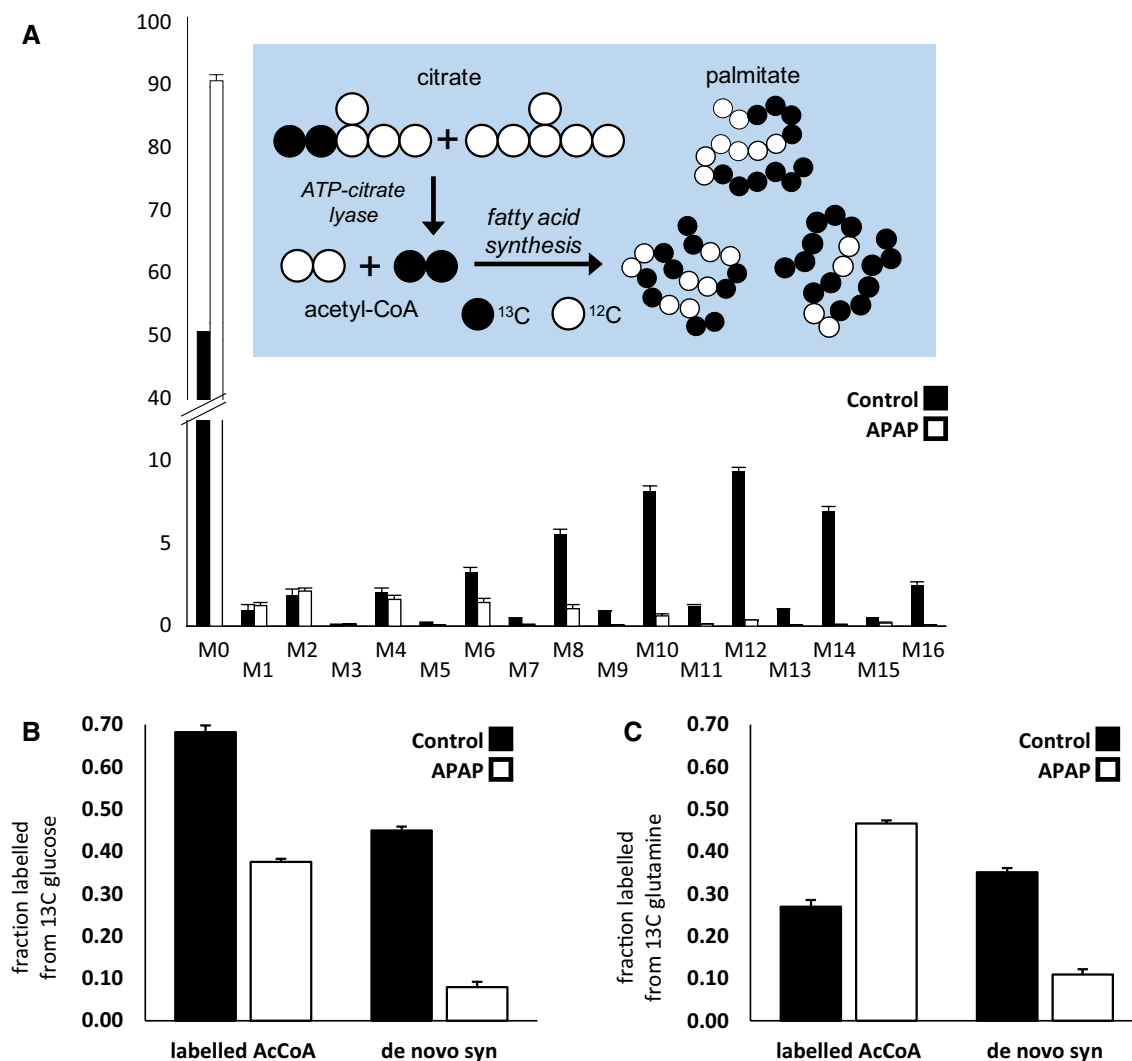

Fig. 3 Isotopologue distributions demonstrate that APAP treatment negatively impacts de novo synthesis of lipids and fatty acids. **a** Mass isotopologue distribution (MID) of palmitate. ISA flux analysis (Keun

and Tredwell 2015, shown here for palmitate) for glucose (**b**) as well as glutamine (**c**) derived carbon. White bars: APAP-treated, black bars: control, $n = 3$

and compared relative fluxes through PPP and glycolysis using 1,2-^{13}C-glucose as a carbon source. In the PPP, the C1 carbon of incoming glucose is released as CO_2 during the conversion of 6-gluconate to ribulose-5-phosphate by 6-phosphogluconate dehydrogenase, meaning that labelled pathway intermediates and down-stream products carry one (or no) ^{13}C-labelled carbons. In contrast, glycolytic intermediates and products carry two (or no) labels when labelled with 1,2-^{13}C-glucose [Fig. 4c, see ref. (Carpenter et al. 2014) for more details]. Lactate, a down-stream product of both pathways, is, therefore, either singly labelled at the C3 position or doubly labelled at C2 and C3, and the relative flux
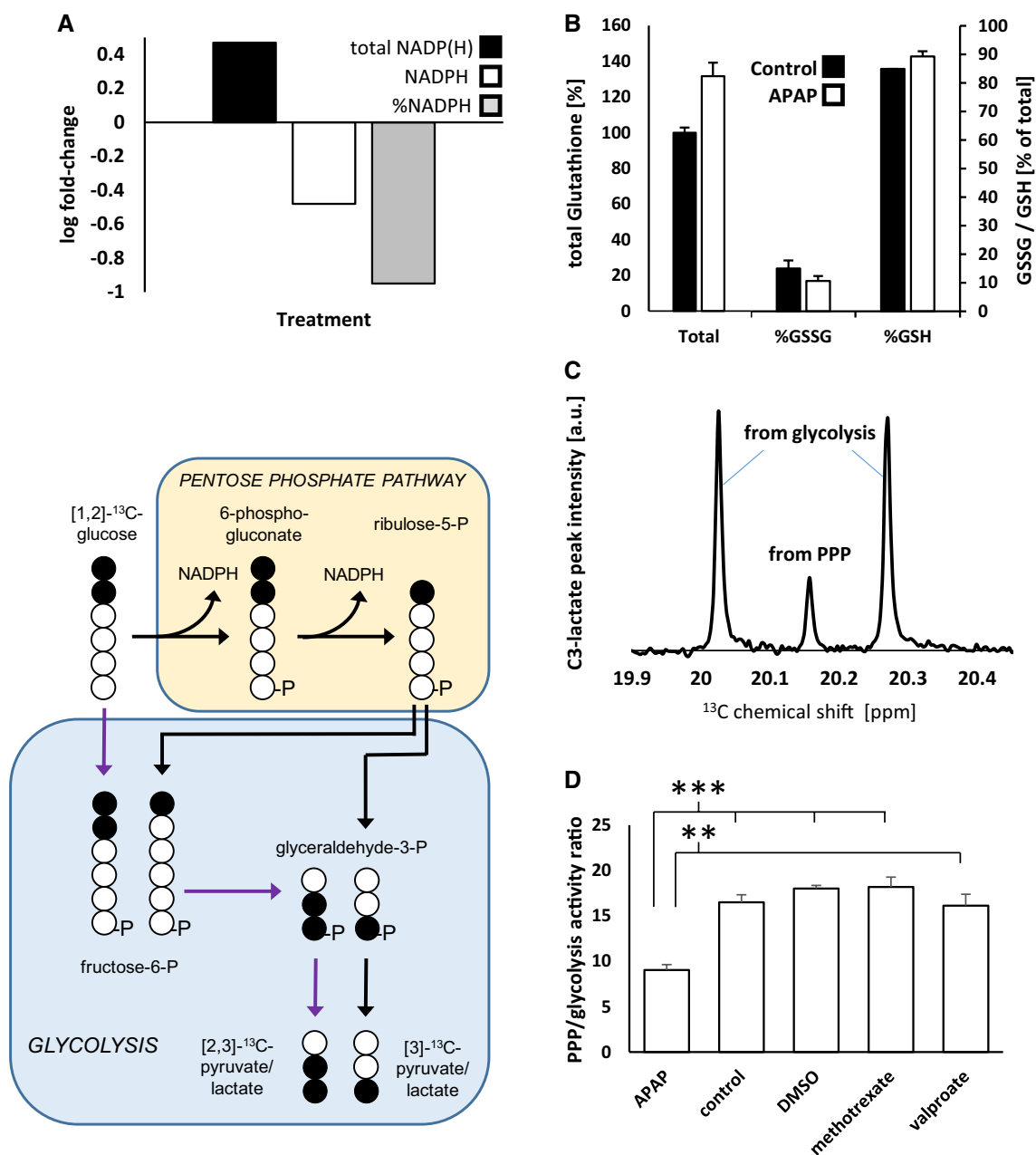

Fig. 4 APAP treatment depletes intracellular NADPH and down-regulates the pentose-phosphate pathway (PPP) in HepG2 cells. a Effect of APAP treatment on NADP(H) level. Bars indicate log$_2$ fold change of HepG2 cells treated with 5 mM APAP for 24 h relative to control; black bar: total NADP(H), white bar: NADPH only, and grey bar: % NADPH of total. b Effect of APAP treatment on glutathione. Bars indicate glutathione in HepG2 cells treated with 5 mM APAP for 24 h relative to control; black bar: control and white bar: APAP. c Representative ^{13}C NMR spectrum derived from supernatants of 1,2-^{13}C glucose-containing media, zoomed to the resonance of the C3 methyl group of lactate. The area of the singlet is proportional to PPP activity; the area of doublet is proportional to glycolysis activity. d Ratios of peak areas from ^{13}C NMR spectra of lactate for the indicated treatments. ***$p < 0.0001$, **$p < 0.001$. (Color figure online)

Table 1 APAP and AZD3965 exhibit mild synergistic effects. Quantification of cell viability, and apoptotic and late apoptotic cells for HepG2 cells co-dosed with AZD3965 and APAP at the concentrations indicated. Each number is the mean of three biological replications. Untreated or treated HepG2 cells were double stained with Annexin V-FITC and PI, and percentage of viable and fraction of apoptotic cells was calculated by flow cytometer, from a total of 5000 events. Annexin V − / PI − were counted as viable cells, whereas Annexin V + / PI − cells were counted as apoptotic

APAP (mM)	0	0.1	0.5	1	2	5
AZD3965 (nM)						
Viable cells (%)						
1000	78	70.63	76.6	65.9	52.93	38.03
100	79.93	75.91	77.7	73.43	65.05	54.05
10	83.4	84.5	83.55	74.9	70.15	57.45
1	87.53	81.15	82.53	78.95	67.55	48.38
0.1	85.63	86.38	85.01	79.48	77.13	63.45
0	83.9	84.75	83.95	73.95	68.5	61.03
Annexin/PI staining (%)						
1000	15.03	19.23	16.97	23.77	30.13	35.97
100	13.73	15.28	15.2	15.68	19.05	26.03
10	11.08	11.7	11.78	15.63	17.48	17.83
1	9.55	13.75	13.1	14.5	19.63	25.38
0.1	10.83	9.48	11.33	12.93	13.15	16.33
0	10.45	10.75	9.45	11.33	13.7	17.68

through PPP and glycolysis can be visualised and quantified by ^{13}C NMR spectroscopy of lactate from cell culture media (Fig. 4c). Comparing cells dosed with APAP to those of cells dosed with different hepatotoxins and untreated controls, we found that relative PPP activity was significantly down-regulated (by 45%, $p > 0.001$, Student's t test) compared to controls and other treatments (Fig. 4d). This observation was consistent with the hypothesis that the reduction in NADPH after APAP exposure is due to a loss of PPP flux and subsequently lower NADPH generation.

As our results indicated that APAP treatment results in growth arrest, reduced fatty acid synthesis, as well as down-regulation of the PPP, we investigated AMPK (phosphorylation) levels, as AMPK activity has been linked to those phenotypes in cancer cells (Jeon et al. 2012). We found the both AMPK as well as phosphorylated AMPK level were unchanged ($p > 0.9$ for both untreated vs. treated comparisons) in response to treatment (Fig. S5).

Increased intracellular production and extra-cellular accumulation of lactate increase the risk to the cell of lactic acidosis, and we hypothesised that this was contributing to cell death with the APAP exposure. To test this hypothesis, we co-dosed HepG2 cells with APAP and AZD3965, an inhibitor of the lactate-exporting monocarboxylate transporter 1, which should result in decreased viability of the cells. To maximise coverage, we treated cells in 36 conditions (see Table 1).

Our data from flow cytometry with annexin V/PI staining suggest that APAP and AZD3965 exert synergistic toxicity on HepG2 cells, particularly at high concentration, whereas, for example, treatment with 5 mM APAP led to a 27% reduction in cell viability compared to untreated controls and dosing with 1 μM AZD3965 only led to a 7% reduction, the combination of the two resulted in a 55% reduction (Table 1). The effect, however, was less pronounced at lower concentrations. Analysis according to Chou and Talalay (Chou and Talalay 1984) confirmed this (not shown). The exacerbated toxicity with AZD3965 was consistent with our hypothesis that APAP-exposed cells are more susceptible to cell death due to intracellular lactic acidosis. In addition, our results from annexin V/PI staining show that cell death follows a mainly apoptotic pattern, as evidenced by cells staining Annexin V + / PI − (Table 1).

Discussion

Metabolic profiling has been a popular tool to describe physiological consequences of toxicity and studies have looked at a variety of biological system and toxins. The physiological effects of APAP toxicity in particular have been analysed multiple times both on a whole-body level in animal models as well as from human biofluids (Tang 2007; O'Connell and Watkins 2010; Coen 2015). Because the pharmacokinetics are well understood and downstream metabolites are easily quantifiable from urine, APAP is often used as a test case for the application of metabolic profiling in contexts as diverse as epidemiology (Loo et al. 2009, 2012) or host–gut microbial interaction microbiology (Klaassen and Cui 2015).
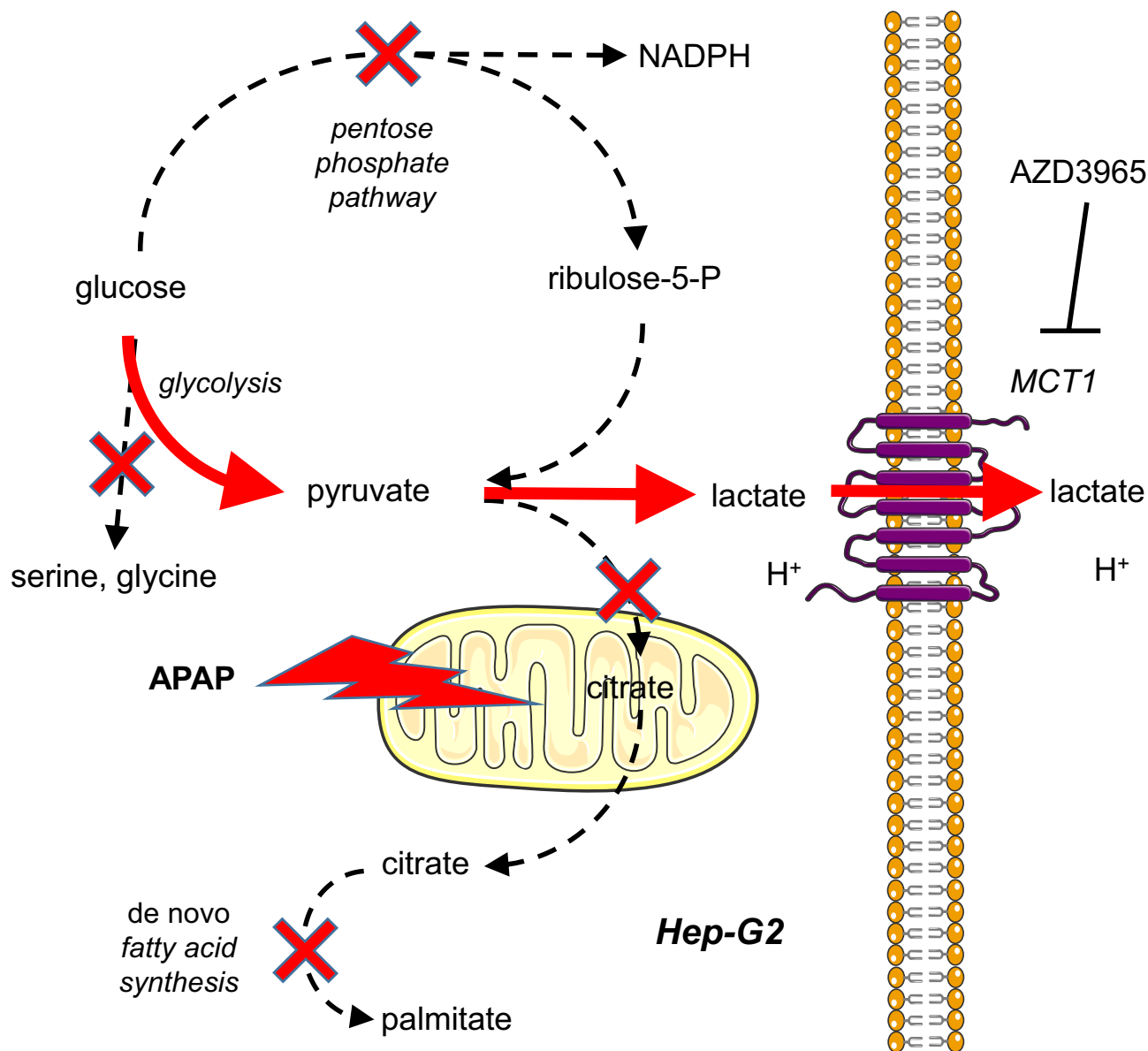
Fig. 5 Model of APAP-induced toxicity in HepG2 cells. Upon APAP exposure, glucose is mostly converted into lactate which is exported by the cells and production of citrate falls. The pentose-phos- phate pathway is down-regulated, resulting in low NADPH levels. Together, this results in low de novo fatty acid synthesis

However, the modelling of chemical toxicology and in particular metabolic processes in vitro is fraught with many challenges, including the use of a proliferating rather than a quiescent cell, limited retention of metabolic activi- ties in immortalised cell lines, and the poor recapitula- tion of the in vivo metabolic environment and substrate availability. Studies of APAP toxicity in hepatoma lines such as HepG2 exemplify this problem very well, since, although it is clear that APAP induces cytotoxicity in this cell line, the type and mechanism of toxicity is likely to be different from that of primary hepatocytes (McGill et al. 2011; Jaeschke et al. 2012; Ramirez et al. 2017), and there

is substantial debate about the relevance to the toxicity observed in humans (Manov et al. 2004; Jaeschke et al. 2012). Yet, the question remains: what are the means by which APAP causes toxicity in this cell line, and what is the role of metabolic processes in this toxicity? The data presented here provide evidence in favour of altered mito- chondrial metabolism and suppression of anabolism being major consequences of toxic doses of APAP in HepG2 cells, and that resulting lactic acidosis may be contributing specifically to cell death.

We found that HepG2 cells die after exposure to high levels of APAP with a dose response similar to that reported

previously (Manov et al. 2004; Raza and John 2015). Conversely, McGill et al. (2011) reported higher resilience to APAP in HepG2. In our data, cell death, as suggested (Jaeschke et al. 2012), follows a (mainly) apoptotic pattern, rather than the necrotic pattern seen for acute cell death in primary liver cells (Hinson et al. 2010). We also found that APAP led to near complete growth arrest, preventing proliferation in vitro.

In our data, we find no evidence for GSH depletion, consistent with the relative paucity in CYP450 enzymes in HepG2 cells that leads to only low levels of NAPQI generation (Jaeschke et al. 2012). Other studies (Manov et al. 2004) have also reported only modest GSH depletion in HepG2 cells for concentrations similar to those used here, despite Raza and John (Raza and John 2015) reporting higher levels of Glutathione S-transferases (GST) in HepG2 cells upon APAP exposure. However, we found that NADPH levels were negatively affected by APAP treatment and this was accompanied by down-regulation of a key NADPH production process, the pentose-phosphate pathway. In consequence, any redox stress subsequent to APAP exposure in HepG2 cells may be due to reduced production of NADPH rather that consumption of reducing equivalents by reactive species.

Using the combinations of stable isotope (^{13}C) tracers, NMR and GC–MS profiling, and isotopomer spectral analysis (ISA), we found that APAP-treated HepG2 cells exhibit an enhanced 'Warburg' effect, in that lactate production from glucose exceeded the already elevated levels of cancer cells, leading to rapid depletion of glucose from the media. Intracellularly, labelling patterns showed a decrease in the proportion of glucose-derived carbon in TCA cycle metabolites in the treated samples compared to controls. While relative flux from glutamine was increased to compensate for this, citrate production was not restored and pool sizes of TCA metabolites were generally lower (Fig. 5). Interestingly, Prill et al. (2016) investigated APAP toxicity in a 3D cell model involving HepG2 cells and found that APAP exposure led to a transient decrease in oxygen uptake and cell death associated with blocking of complex III of the electron transport chain (ETC). Such inhibition of the ETC causes NADH accumulation and feedback inhibition of the TCA cycle enzymes and pyruvate dehydrogenase which could explain reduced entry of glucose-derived pyruvate into the TCA cycle.

We also found that de novo fatty acid synthesis was severely negatively impacted by the APAP treatment. This finding is echoed in the other studies using metabolic profiling to investigate APAP toxicity. A recent study investigating HepaRG cells (Van den Eede et al. 2015) found a decrease in unsaturated phospholipids upon treatment. While HepaRG are thought to be physiologically 'closer' to primary hepatocytes and have higher CYP2E1 expression (McGill et al. 2011), the fact that similar metabolic pathways are affected

by APAP exposure in both models is interesting. This inhibition of fatty acid synthesis could be due to the reduced capacity after APAP treatment of mitochondria to produce citrate, the source of cytosolic acetyl-CoA which is the carbon source for de novo synthesised fatty acids. Alternatively, this could be explained by the drop in NADPH levels, as fatty acid synthesis is also a major consumer of NADPH.

High levels of anabolism, particularly de novo lipogenesis (Currie et al. 2013) and NADPH production, are a requirement for rapid proliferation of cancer cells as observed for HepG2 cells in culture. Therefore, the inhibition of these processes by APAP could be a key contributor to the reduced proliferation in this cell model observed with the APAP treatment. Furthermore, these metabolic responses may be specifically relevant to proliferating cells and not quiescent primary cells. While it was not possible to determine from our experiments whether the loss of NADPH and lipogenesis was consequential to the loss of mitochondrial metabolism, we did not see the activation of the AMPK pathway which normally suppresses NADPH and fatty acid production if ATP levels fall (Jeon et al. 2012). This implies that the loss of citrate and NADPH production is a more significant factor in the inhibition of anabolism than a loss of energy production. Furthermore, while the increase in glycolytic rate observed could compensate for loss of mitochondrial ATP production, it possibly comes at the cost of PPP-driven NADPH production and, thus, biosynthesis and growth.

Combinatorial dosing with the MCT-1 inhibitor AZD3965 leads to increased cell death in HepG2 cells, implying that excessive lactate production was contributing to cell death in this model. Other studies have shown that the anti-cancer effects of AZD3965 can be enhanced by combination with respiratory inhibitors such as metformin (Marchiq et al. 2015; Noble et al. 2017; Beloueche-Babari et al. 2017), which further supports the inhibition of mitochondrial respiration as the initiating event of APAP toxicity in HepG2 cells despite the lack of NAPQI generation. Both agonistic and antagonistic interactions with high-dose acetaminophen have been described with the other therapeutics. For example, high-dose APAP suppresses the activity of doxorubicin, a common chemotherapeutic (Manov et al. 2007). Conversely, two drugs used in treatment of tuberculosis, rifampicin and isoniazid, have been reported to increase APAP toxicity (Nicod et al. 1997), though the mechanism remains to be elucidated. Lactic acidosis has been observed as an important early event in human overdose of APAP, prior to hepatocellular toxicity (Shah et al. 2011). However, the model system used here is not appropriate to extrapolate to this phenomenon and further work is needed to evaluate the relevance of the mechanisms defined in HepG2 cells to the clinical setting.

Our data show that APAP and AZD3965 exhibit synergistic properties, particularly at high-dose, suggesting that the

metabolic changes associated with APAP exposure enhance the efficacy of MCT-1 inhibition.

Limitations and future work

Our study points to a potential oxidative stress-independent impact of APAP on hepatoma physiology. While we propose a model involving glycolysis and the TCA cycles, further measurement, for example, direct measurements of ETC activity in isolated mitochondria or markers of cell cycle could be carried out to compile further evidence. As stated above, HepG2 cells differ from many hepatoma lines in their low CYP2E1 expression. Studies in other hepatoma cell lines with low CYPE1 expression, such as Hep3B cells, would strengthen our finding of NAPQI-independent cell death from APAP. Moreover, studies with cell lines with higher CYPE1 expression, such as primary hepatocytes, HepaRG (McGill et al. 2011), or artificial induction of CYP450 enzymes (Gerets et al. 2012), could be employed to investigate the general applicability of our findings.

In this study, we describe the impact of APAP toxicity on de novo fatty acid synthesis. This, of course, falls short characterising the impact in the whole lipid pool. It would, therefore, be beneficial to employ a full lipidomic approach to characterise the impact of APAP on this compound class. In our discussion, we present a model explaining the impact of APAP on the NADPH pool and lactate production. In the future, further mechanistic studies are need to fully elucidate how APAP manages to alter metabolic flux, which proteins it binds and why the cells are driven into an enhanced Warburg effect. Importantly, the signalling cascade leading to growth arrest needs to be elucidated.

Conclusion

Our data show that APAP leads to severe metabolic alterations in the HepG2 cell line, negatively impacting proliferating capacity and providing an oxidative stress-independent mechanism for killing of hepatoma cell lines.

References

Beckonert O, Keun HC, Ebbels TMD et al (2007) Metabolic profiling, metabolomic and metabonomic procedures for NMR spectroscopy of urine, plasma, serum and tissue extracts. Nat Protoc 2:2692–2703. https://doi.org/10.1038/nprot.2007.376

Behrends V, Tredwell GD, Bundy JG (2011) A software complement to AMDIS for processing GC-MS metabolomic data. Anal Biochem 415:206–208

Beloueche-Babari M, Wantuch S, Casals Galobart T et al (2017) MCT1 Inhibitor AZD3965 increases mitochondrial metabolism, facilitating combination therapy and noninvasive magnetic resonance Spectroscopy. Cancer Res 77:5913–5924. https://doi.org/10.1158/0008-5472.CAN-16-2686

Bunchorntavakul C, Reddy KR (2013) Acetaminophen-related hepatotoxicity. Clin Liver Dis 17:587–607. https://doi.org/10.1016/j.cld.2013.07.005

Carpenter KLH, Jalloh I, Gallagher CN et al (2014) (13)C-labelled microdialysis studies of cerebral metabolism in TBI patients. Eur J Pharm Sci 57:87–97. https://doi.org/10.1016/j.ejps.2013.12.012

Chou TC, Talalay P (1984) Quantitative analysis of dose-effect relationships: the combined effects of multiple drugs or enzyme inhibitors. Adv Enzyme Regul 22:27–55

Coen M (2015) Metabolic phenotyping applied to pre-clinical and clinical studies of acetaminophen metabolism and hepatotoxicity. Drug Metab Rev 47:29–44. https://doi.org/10.3109/03602532.2014.982865

Currie E, Schulze A, Zechner R et al (2013) Cellular fatty acid metabolism and cancer. Cell Metab 18:153–161. https://doi.org/10.1016/j.cmet.2013.05.017

Dai Y, Cederbaum AI (1995) Cytotoxicity of acetaminophen in human cytochrome P4502E1-transfected HepG2 cells. J Pharmacol Exp Ther 273:1497–1505

Gerets HHJ, Tilmant K, Gerin B et al (2012) Characterization of primary human hepatocytes, HepG2 cells, and HepaRG cells at the mRNA level and CYP activity in response to inducers and their predictivity for the detection of human hepatotoxins. Cell Biol Toxicol 28:69–87. https://doi.org/10.1007/s10565-011-9208-4

Hanahan D, Weinberg RA (2011) Hallmarks of cancer: the next generation. Cell 144:646–674. https://doi.org/10.1016/j.cell.2011.02.013

Hinson JA, Roberts DW, James LP (2010) Mechanisms of acetaminophen-induced liver necrosis. Handb Exp Pharmacol. https://doi.org/10.1007/978-3-642-00663-0_12

Jaeschke H, Williams CD, McGill MR (2012) Caveats of using acetaminophen hepatotoxicity models for natural product testing. Toxicol Lett 215:40–41. https://doi.org/10.1016/j.toxlet.2012.09.023

Jeon S-M, Chandel NS, Hay N (2012) AMPK regulates NADPH homeostasis to promote tumour cell survival during energy stress. Nature 485:661–665. https://doi.org/10.1038/nature11066

Kind T, Wohlgemuth G, Lee DY et al (2009) FiehnLib: mass spectral and retention index libraries for metabolomics based on quadrupole and time-of-flight gas chromatography/mass spectrometry. Anal Chem 81:10038–10048. https://doi.org/10.1021/ac9019522

Klaassen CD, Cui JY (2015) Review: mechanisms of how the intestinal microbiota alters the effects of drugs and bile acids. Drug Metab Dispos 43:1505–1521. https://doi.org/10.1124/dmd.115.065698

Loo RL, Coen M, Ebbels T et al (2009) Metabolic profiling and population screening of analgesic usage in nuclear magnetic resonance spectroscopy-based large-scale epidemiologic studies. Anal Chem 81:5119–5129. https://doi.org/10.1021/ac900567e

Loo RL, Chan Q, Brown IJ et al (2012) A comparison of self-reported analgesic use and detection of urinary ibuprofen and acetaminophen metabolites by means of metabonomics: the INTERMAP

Study. Am J Epidemiol 175:348–358. https://doi.org/10.1093/aje/kwr292

Macanas-Pirard P, Yaacob N-S, Lee PC et al (2004) Glycogen synthase kinase-3 mediates acetaminophen-induced apoptosis in human hepatoma cells. J Pharmacol Exp Ther 313:780–789. https://doi.org/10.1124/jpet.104.081364

Manov I, Hirsh M, Iancu TC (2002) Acetaminophen hepatotoxicity and mechanisms of its protection by *N*-acetylcysteine: a study of Hep3B cells. Exp Toxicol Pathol 53:489–500. https://doi.org/10.1078/0940-2993-00215

Manov I, Hirsh M, Iancu TC (2004) N-Acetylcysteine does not protect HepG2 cells against acetaminophen-induced apoptosis. Basic Clin Pharmacol Toxicol 94:213–225. https://doi.org/10.1111/j.1742-7843.2004.pto940504.x

Manov I, Bashenko Y, Eliaz-Wolkowicz A et al (2007) High-dose acetaminophen inhibits the lethal effect of doxorubicin in HepG2 cells: the role of P-glycoprotein and mitogen-activated protein kinase p44/42 pathway. J Pharmacol Exp Ther 322:1013–1022. https://doi.org/10.1124/jpet.107.121772

Marchiq I, Le Floch R, Roux D et al (2015) Genetic disruption of lactate/H + symporters (MCTs) and their subunit CD147/BASIGIN sensitizes glycolytic tumor cells to phenformin. Cancer Res 75:171–180. https://doi.org/10.1158/0008-5472.CAN-14-2260

McGill MR, Jaeschke H (2013) Metabolism and disposition of acetaminophen: recent advances in relation to hepatotoxicity and diagnosis. Pharm Res 30:2174–2187. https://doi.org/10.1007/s11095-013-1007-6

McGill MR, Yan H-M, Ramachandran A et al (2011) HepaRG cells: a human model to study mechanisms of acetaminophen hepatotoxicity. Hepatology 53:974–982. https://doi.org/10.1002/hep.24132

Millard P, Letisse F, Sokol S, Portais J-C (2012) IsoCor: correcting MS data in isotope labeling experiments. Bioinformatics 28:1294–1296. https://doi.org/10.1093/bioinformatics/bts127

Nicod L, Viollon C, Regnier A et al (1997) Rifampicin and isoniazid increase acetaminophen and isoniazid cytotoxicity in human HepG2 hepatoma cells. Hum Exp Toxicol 16:28–34. https://doi.org/10.1177/0960327197016001061

Noble RA, Bell N, Blair H et al (2017) Inhibition of monocarboxylate transporter 1 by AZD3965 as a novel therapeutic approach for diffuse large B-cell lymphoma and Burkitt lymphoma. Haematologica 102:1247–1257. https://doi.org/10.3324/haematol.2016.163030

O'Connell TM, Watkins PB (2010) The application of metabonomics to predict drug-induced liver injury. Clin Pharmacol Ther 88:394–399. https://doi.org/10.1038/clpt.2010.151

Prill S, Bavli D, Levy G et al (2016) Real-time monitoring of oxygen uptake in hepatic bioreactor shows CYP450-independent mitochondrial toxicity of acetaminophen and amiodarone. Arch Toxicol 90:1181–1191. https://doi.org/10.1007/s00204-015-1537-2

Ramirez T, Strigun A, Verlohner A et al (2017) Prediction of liver toxicity and mode of action using metabolomics in vitro in HepG2 cells. Arch Toxicol. https://doi.org/10.1007/s00204-017-2079-6

Raza H, John A (2015) Differential cytotoxicity of acetaminophen in mouse macrophage J774.2 and human hepatoma HepG2 cells: protection by diallyl sulfide. PLoS One 10:e0145965. https://doi.org/10.1371/journal.pone.0145965

Shah AD, Wood DM, Dargan PI (2011) Understanding lactic acidosis in paracetamol (acetaminophen) poisoning. Br J Clin Pharmacol 71:20–28. https://doi.org/10.1111/j.1365-2125.2010.03765.x

Stein SE (1999) An integrated method for spectrum extraction and compound identification from gas chromatography/mass spectrometry data. J Am Soc Mass Spectrom 10:770–781. https://doi.org/10.1016/S1044-0305(99)00047-1

Stincone A, Prigione A, Cramer T et al (2015) The return of metabolism: biochemistry and physiology of the pentose phosphate pathway. Biol Rev Camb Philos Soc 90:927–963. https://doi.org/10.1111/brv.12140

Tang W (2007) Drug metabolite profiling and elucidation of drug-induced hepatotoxicity. Expert Opin Drug Metab Toxicol 3:407–420. https://doi.org/10.1517/17425255.3.3.407

Tredwell GD, Keun HC (2015) convISA: simple, convoluted method for isotopomer spectral analysis of fatty acids and. Metab Eng. https://doi.org/10.1016/j.ymben.2015.09.008

Van den Eede N, Cuykx M, Rodrigues RM et al (2015) Metabolomics analysis of the toxicity pathways of triphenyl phosphate in HepaRG cells and comparison to oxidative stress mechanisms caused by acetaminophen. Toxicol In Vitro 29:2045–2054. https://doi.org/10.1016/j.tiv.2015.08.012

Vander Heiden MG, Cantley LC, Thompson CB (2009) Understanding the Warburg effect: the metabolic requirements of cell proliferation. Science 324:1029–1033. https://doi.org/10.1126/science.1160809

Wishart DS, Tzur D, Knox C et al (2007) HMDB: the human metabolome database. Nucleic Acids Res 35:D521–D526. https://doi.org/10.1093/nar/gkl923

Yoon E, Babar A, Choudhary M et al (2016) Acetaminophen-induced hepatotoxicity: a comprehensive update. J Clin Transl Hepatol 4:131–142. https://doi.org/10.14218/JCTH.2015.00052